IIETA International Information and Engineering Technology Association
Advancing the World of Information and Engineering

Journal of New Materials for Electrochemical Systems
Vol. 26, No.4, October 2023, pp. 312-321
Journal homepage: http://iieta.org/journals/jnmes

Tuning the Particle Size Distribution at Cathode for Enhanced Li-Ion Battery Performance

Brajesh Kumar Kanchan[1,2], Pitambar Randive[1*]

[1] Department of Mechanical Engineering, National Institute of Technology Silchar, Silchar, Assam-788010, India
[2] Department of Production Engineering, PSG College of Technology, Coimbatore, Tamilnadu-641004, India

Corresponding Author Email: pitambar@mech.nits.ac.in (P. Randive)

https://doi.org/10.14447/jnmes.v26i4.a10

Received: January 10, 2023
Accepted: July 04, 2023

Keywords:
Li-ion battery, Functional electrode, Cathode particle size distribution, Ultrafast charging, Specific power, Loss characteristics.

ABSTRACT

The Li-ion battery's diverse applications necessitate the quest to design energy and power-dense electrode microstructure. The present study uses the Doyle-Newman framework to probe the interplay of cathode particle size configurations for various current densities. Our study reveals the interplay of cathode particle size distribution and C-rate on cell performance characteristics. Further, the cell performs better when the cathode employs a cathode particle size configuration arranged non-uniformly. Moreover, the cell characteristics, viz. specific energy, specific power, and capacity, are highest for the configuration where the cathode particle size increases in the direction of the cathode current collector interface. Additionally, losses are relatively lesser in this configuration. Furthermore, the cell characteristics become more significant for higher current density. In addition, as particle size grows at a higher rate, the improvement in cell performance is significant. Our findings bear utility towards advancement in cathode on the microstructural scale and offer better spatiotemporal ionic transport kinetics.

NOMENCLATURE

r	Particle radius, m
D	Salt diffusion coefficient, m^2/s
U	Open circuit potential, V
t_+^0	Transference number
b	Bruggeman coefficient for tortuosity
$\mathcal{E}$	Electrode volume fraction
c	Salt concentration, mol/m^3
$ø$	Electric potential, V
J_{Li}	Current density, A/m^2
a	Interfacial area per unit volume, m^2/m^3
J_{Li0}	Reference exchange current density, A/m^2
Q_0	Initial Capacity, Ah/kg
L_a	Length of anode, m
T	Cell temperature, K
σ	Active material conductivity, S/m
k	Ionic conductivity, S/m
α	transfer coefficient
R_s	Active material particle radius, m
t	Time, s
L_{sep}	Length of separator, m
L_c	Length of cathode, m
τ	Tortuosity

Subscripts

a	Anode
c	Cathode
sep	Separator
e	Electrolyte phase
s	Solid-phase
0	Initial condition
D	Diffusion
ch	Charge
$disch$	Discharge

Superscript

max	Maximum
min	Minimum
eff	Effective

1. INTRODUCTION

The pursuit of affordable and cleaner energy increases with stringent environmental regulations implemented worldwide on the recommendation of the United Nations [1]. Lithium-ion (Li-ion) technology adds a much-needed reliability feature to affordable, cleaner energy sources to enlarge the application and allow mass usage. Li-ion is an optimal energy storage device with high power and energy density characteristics [2,3]. Its current energy and power density are enough to support the consumer electronic market very well, whereas it has to show exponential growth in power and energy density to outrun the oil-based transportation sector and advance to the aviation sector [3,4]. Operating at high power and energy could compromise cycle life and safety aspects as several non-linear multiphysics related to spatiotemporal electrochemical and transport reactions are still unanswered [5–7]. To overcome the electrochemical and thermodynamic limitations, one can use alternating material selection for different cell components [8]. Another approach to increase theoretical

capacity at greater current densities could be an innovative porous functional electrode microstructure that promotes efficient ionic transport with the same materials [9]. At the microstructural level, active material configurations allow electronic transport and passively promote ionic transport through the pores, thereby influencing electrochemical performance parameters [10–13]. Furthermore, it can be noted that real electrodes are made up of non-uniform microstructure distribution [14]. Assuming all electrode particles as equal and uniform is an oversimplification with developed computational facilities. Moreover, there is substantial uncertainty about the ideal porous non-uniform electrode configurations that optimally use ionic and electronic transport for higher current density operation. Consequently, a focused research endeavor is necessary to enhance the comprehension of ionic transport by thoroughly understanding the consequences of customized electrode microstructure on performance characteristics.

The microstructural aspect of the porous electrode is majorly investigated based on porosity, tortuosity, and particle size distribution. Fuller et al. [15] conducted groundbreaking research examining the intercalation mechanism within electrodes and revealed that thinner cells are optimal in case of higher current density. Furthermore, Mukherjee et al. [16] probed electrode kinetics and established a numerical model for cell performance prediction. Newman and team [15,17–19] proposed a porous electrode model using a concentrated solution framework. Baade et al. [20] described the quantification procedure for particle orientation in porous graphite electrodes. Hosseinzadeh et al. [21] studied the effect of customized porosity and noted lesser heat generation than uniform porosity. Bae et al. [22] investigated intercalation characteristics in dual-porosity electrodes and found that specific capacity is maximum for dual porosity. Wood and Ebner [23] analyzed electrode formation with magnetic orientation and observed significantly higher capacity, later verified by Billaud et al. [24]. Peterson and Wheeler [25] stated that electronic transport is a strong function of electrode microstructure characteristics. Ramadesigan et al. [26] examined customized electrodes, emphasizing ohmic overpotential. They observed a significant reduction of 18% in the ohmic drop when utilizing a customized microstructure. Hur et al. [27] analyzed three-dimensional micro batteries using photopatterning for higher energy density. Pikul et al. [28] found that micro batteries with nonporous electrodes yield significantly higher power densities.

Particle size distribution dictates the transport characteristics of lithium-ion batteries. Suthar et al. [29] reported the least capacity fade could be achieved by reducing the active material near the interface of the anode and separator. The dimension of the electrode active material range varies from 10^{-9} to 10^{-6} m [30,31]. Moreover, smaller anode particle achieves higher cell performance [32]. Park and Lee [33] analyzed the relationship between particle configuration and SEI (stands for “solid electrolyte interphase”). They have observed higher SEI heat in the case of smaller anode particles.

Sacken et al. [34] discussed thermal stability and emphasized the importance of anode microstructure in maintaining thermal safety. Later, Tran et al. [35] examined particle size distribution's influence and advocated using smaller particles for better cell performance. Furthermore, Meyer et al. [36] noted faster oxidation for smaller anode particles. Ali et al. [37] concluded that stress concentration is higher for smaller particles and higher current density. Du et al. [38] suggested a correlation between particle configuration, cycling rate, and diffusivity. They showed that the specific energy decreases with an increase in particle size.

The earlier investigations on Li-ion cells have largely considered uniform particle considerations for slow and fast discharging-charging characteristics. Although few studies recently reported the interplay of non-uniform microstructure, they have mainly focused on evaluating non-uniform microstructure in one electrode and assumed other electrodes with uniform characteristics [14,19,39,40]. Furthermore, the effect of ultrafast charging-discharging has mostly been overlooked for non-uniform electrode particle size distribution. Herein, one can note that electrochemical reactions at porous electrodes are a two-way transport process for electrons and ions. Additionally, charging and discharging characteristics exhibit different spatiotemporal electrochemical and transport properties due to different anode and cathode materials. Moreover, recent development in manufacturing technology enables customized nanostructured electrode skeletons with improved redox reactions [41–44]. Hence, it should be noted that a few questions were overlooked, as follows:

a) What are the effects of non-uniform cathode particle configurations?
b) How do loss characteristics, especially overpotential and power dissipation density, depend on particle size distribution?
c) How is the size of cathode particle distribution correlated with charging and discharging characteristics, particularly for a higher C rate?

Therefore, the current research investigates the interplay of cathode particle size configurations probed for various current densities to answer the above questions. Moreover, the capacity, specific energy, specific power, and overpotential characteristics are discussed for various cathode particle distributions. Herein, it can be noted that estimating complex spatiotemporal dynamics of ionic transport in Li-ion batteries is one of three challenges for next-generation battery management related to automated electric vehicles [45]. Note that the usability of the lithium-ion battery to its full potential needs an in-depth probing of performance characteristics [46] to enhance the use of active material participation in electrochemical reactions.

The paper is divided into several sections, organized in the following manner. Section 2 offers an overview of the problem statement, including the governing equations and boundary conditions. Section 3 details the numerical methodology that was employed. Section 4 focuses on the validation process conducted for the utilized model. Section 5 presents the results obtained from the present study. Finally, section 6 encompasses the conclusions drawn from the research.

2. PROBLEM FORMULATION

The problem formulation section delineates the physical model employed to bridge the literature gap, its governing equations, and boundary conditions. In this context, it can be noted that the present study considered the Doyle-Newman framework model and assessed different non-uniform cathode particle size distributions over cathode length (referred to as Cases), as shown in Fig. 1. It is well known that the assumption of considering uniform particle size distribution is a bit of

oversimplification to simplify the complex electronic and ionic spatiotemporal kinetics. In fact, heterogeneous particle size distribution in the electrode is more realistic and practical than found in Li-ion cells due to manufacturing constraints [14,19]. This non-uniformity in particle size distribution in porous electrodes likely induces variation in transport characteristics.

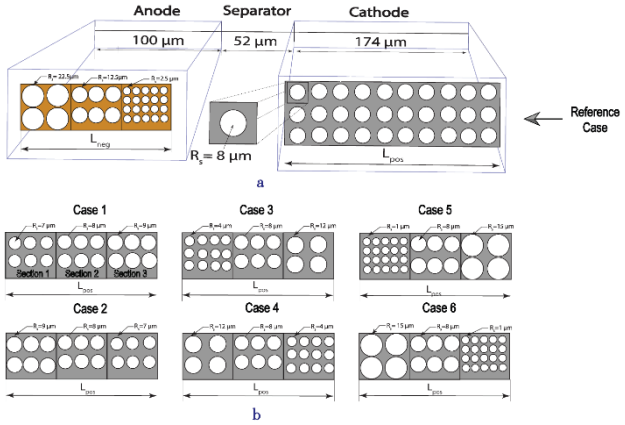

Figure 1: Schematic of Lithium-ion cell model: (a) reference case with the uniform particle size distribution of cathode, and (b) different cathode non-uniform particle size configurations (Cases).

Note that the "Reference Case" is the one in which particle size distribution is uniform at the cathode, while the anode particle distribution is taken non-uniform and adopted from our earlier work [47]. Herein, it can be noted from Fig. 1b that although the various configuration presents different cathode particle radius across the cathode length scale, the average particle radius (R_s) is kept constant and equal to 8 µm. Furthermore, Case 1, Case 3, and Case 5 depict the cathode particle distribution in increasing particle radius with variation (Δr = 1µm, 4 µm, and 7 µm), respectively. On the contrary, Case 2, Case 4, and Case 6 depict the cathode particle distribution in decreasing particle radius with variation (Δr = 1µm, 4 µm, and 7 µm), respectively, as shown in Fig. 1(b).

The cell is considered to be fully charged at the initial condition. No side reactions are taken into account. Further, edge influences are also not taken following the work of Doyle et al. [17]. Lithiated-Graphite (LiC_6) and Lithium-Manganese Oxide ($LiMn_2O_4$) are implied as anode and cathode material with Lithium hexafluorophosphate (LiPF6) as electrolyte. The volume fraction of salts, i.e., Ethylene Carbonate (EC) and Dimethyl Carbonate (DMC), are in 1:2 proportion. The average radius of active material is 12.5 µm and 8 µm for the anode and cathode, respectively. Spherical active materials are assumed [17]. The values of characteristics, parameters, and dimensions of the computational domain are taken [17], as presented in Table 1.

Table 1: Electrode materials and parameters

Parameter (unit)	**Anode**	**Cathode**
$\mathbf{D_s}$ (m^2/s)	3.9×10^{-14}	1.0×10^{-13}
$\boldsymbol{\sigma_0}$ (S/m)	100	3.8
$\mathbf{c_{max}}$ (mol/m^3)	26,390	22,860
ρ (kg/m^3)	2,328.50	1,347.33
L (µm)	100	174
$\mathbf{R_s}$ (µm)	12.5	8
$\mathbf{c_{ref}}$ (mol/m^3)	14,870	3,900
Ɛ	0.357	0.444

The maximum discharge capacity, aerial capacity, and current density are assumed to be 44.7 mAh, 18.3Ah/m2, and 17.5 A/m2, respectively. Moreover, the capacity ratio is considered as 1.7 [17]. It is imperative to note that the Li-ion battery's electrochemical characteristics depend on the current density applied [14]. Therefore, the present study evaluates the cell performance at 0.3C, 1C, and 10C, respectively.

2.1. Governing Equations

The Doyle-Newman framework model, based on porous electrode theory, describes the material transport in electrodes and electrolytes [48,49].

$$\frac{\partial c_s}{\partial t} = \frac{D_s}{r^2}\frac{\partial}{\partial r}\left(r^2\frac{\partial c_s}{\partial r}\right) \quad (1)$$

$$\varepsilon_e\frac{\partial c_e}{\partial t} = \frac{\partial}{\partial x}\left(D_e^{eff}\frac{\partial}{\partial x}c_e\right) + \frac{(1-t_+^0)}{F}j_{Li} \quad (2)$$

$$\frac{\partial}{\partial x}\left(\sigma^{eff}\frac{\partial}{\partial x}\phi_s\right) = j_{Li} \quad (3)$$

$$\frac{\partial}{\partial x}\left(k^{eff}\frac{\partial}{\partial x}\phi_e\right) + \frac{\partial}{\partial x}\left(k_D^{eff}\frac{\partial}{\partial x}lnc_e\right) + j_{Li} = 0 \quad (4)$$

Where $c, D, \varepsilon, t_+^0, k, j_{Li}, \sigma$ denotes lithium concentration, diffusion coefficient, porosity, transference number, ionic conductivity, current density, and solid conductivity, respectively.

The correlation between current density and overvoltage is described by Butler-Volmer electrode kinetics as

$$j_{Li} = j_{Li_0}\left[exp\left(\frac{\alpha_a F}{2RT}(\phi_s - \phi_e - U)\right) - exp\left(-\frac{\alpha_c F}{2RT}(\phi_s - \phi_e - U)\right)\right] \quad (5)$$

Where $j_{Li_0}, \alpha, F, R, T, U$ shows exchange current density, transfer coefficient, Faraday's Constant, Universal gas constant, and open circuit potential, respectively.

2.2. Boundary Conditions

The following are the boundary conditions for the present computational domain [49].

$$\left.\frac{\partial c_e}{\partial x}\right|_{x=0} = \left.\frac{\partial c_e}{\partial x}\right|_{x=L} = 0 \quad (6)$$

$$\left.\frac{\partial \phi_e}{\partial x}\right|_{x=0} = \left.\frac{\partial \phi_e}{\partial x}\right|_{x=L} = 0 \quad (7)$$

$$-\sigma_-^{eff}\left.\frac{\partial \phi_s}{\partial x}\right|_{x=0} = \sigma_+^{eff}\left.\frac{\partial \phi_s}{\partial x}\right|_{x=L} = \frac{I}{A} \quad (8)$$

$$\left.\frac{\partial \phi_s}{\partial x}\right|_{x=L_n} = \left.\frac{\partial \phi_s}{\partial x}\right|_{x=L_n+L_{sep}} = 0 \quad (9)$$

$$\left.\frac{\partial c_s}{\partial r}\right|_{r=0} = 0, -D_s\left.\frac{\partial c_s}{\partial r}\right|_{r=R_s} = \frac{j^{Li}}{a_s F} \quad (10)$$

The electrochemical analysis consists of specific power, specific energy, overpotential, and power dissipation density. The overpotential generated due to activation, ohmic, and concentration can be expressed as

$$\eta = (\phi_s - \phi_e - U) \quad (11)$$

where ϕ_s, ϕ_e, U shows the electrical potential of solid and electrolyte and open circuit potential. Power dissipation density is denoted as a summation of reversible and irreversible losses as

$$Q_{Pdd} = \left(j_{Li_0} \times a_s \times \Delta t \times \frac{dU}{dT}\right) + \left(j_{Li_0} \times a_s \times \eta\right) \quad (12)$$

Specific energy refers to the quantity of electrical energy stored per kilogram of battery mass. [6] and is denoted as

$$S.E. = \frac{min(Q_c,Q_a)\times(U_c-U_a)}{M_t} \quad (13)$$

Where Q, M_t denotes capacity and total mass, respectively. Further, Specific power denotes the measure of power obtained per kilogram of battery mass. [6].

$$S.P = \frac{\int_{t_0}^{t_f} I(t)\times U(t)dt}{(t_f-t_0)\times M_t} \quad (14)$$

Where t_o, t_f are starting time and end time for cell charging or discharging, respectively.

3. NUMERICAL PROCEDURE

A mathematical framework for non-uniform cathode particle size distribution is discussed in this section. The governing equations (1-5) described earlier have been numerically solved using the finite element method. Initially, the 1D domain is segregated into line segments. For each line segment, the electrolyte salt concentration (c), solid-phase potential ($ø_s$), and electrolyte potential ($ø_e$) are considered primary variables. These primary variables are approximated through interpolation. The approximation for the primary variables in each line segment is given by:

$$C = \sum_{e=1}^{N^C} \varphi_e^C C_e, \emptyset_s = \sum_{e=1}^{N^{\emptyset_s}} \varphi_e^{\emptyset_s} \emptyset_{se}, \emptyset_e = \sum_{e=1}^{N^{\emptyset_e}} \varphi_e^{\emptyset_e} \emptyset_e \quad (15)$$

Here, $\varphi_e^C, \varphi_e^{\emptyset_s}, \varphi_e^{\emptyset_e}$ represent the shape functions for electrolyte salt concentration, solid-phase potential, and electrolyte potential, respectively. Additionally, C, $ø_s$, and $ø_l$ denote variables at different nodes. The governing equations, originally in partial differential equations, used Galerkin weighted residual methods and converted them into integral equations. The variables are substituted into these integral equations, resulting in a residual that is equated to zero to form the local matrix. The local matrices are then assembled into the global matrix. Moreover, the boundary conditions are applied. A conjugate gradient-based PARDISO solver is used in this study to determine the variables. The solution is considered converged when the computational error falls within the specified tolerance limit of 10^{-3}.

4. MODEL VALIDATION

Before presenting the results and discussing the findings for non-uniform cathode particle size distribution, a model validation process is carried out to ensure the accuracy and reliability of the methodology employed in this study. Hence, the accuracy of the solver in capturing the intricacy of spatiotemporal reaction kinetics in Li-ion cells is confirmed by comparing the cell potential Doyle et al. [17] considered $\varepsilon_a = 0.357, \varepsilon_c = 0.444$ as the porosity of anode and cathode, respectively. Similarly, the present study also considered the same values.

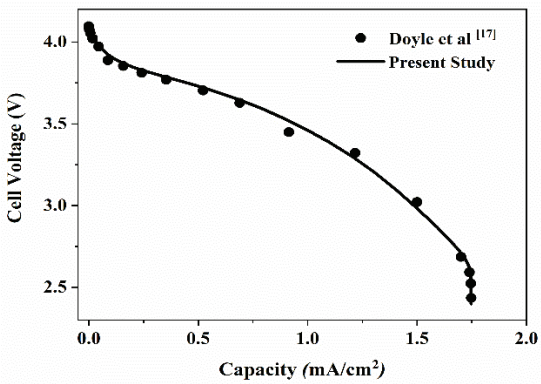

Figure 2: Model validation: comparison of capacity variation with experimental results of Doyle et al. [17].

A close agreement can be observed between the results obtained by the solver employed with the experimental work of Doyle et al. [17], which thus confirms the accuracy.

5. RESULT AND DISCUSSION

The present study analyzes the effects of tuning the particle size distribution at the cathode on various battery performance metrics, particularly for slow, fast, and ultrafast charging-discharging processes. Initially, a capacity comparison is conducted to demonstrate the substantial enhancement in cell performance resulting from the non-uniform cathode particle distribution. Thereafter, the cell performance characteristics, viz. specific energy, specific power, and capacity, are discussed for non-uniform cathode particle distributions. Moreover, the electrochemical loss characteristics, i.e., overpotential and power dissipation density, are also analyzed in the subsequent sections.

5.1 Improvement in Capacity with Non-Uniform Particle Size Distribution at the Cathode: Comparison with Existing Works

The transport characteristics in Li-ion cells are affected by microstructural attributes, viz. porosity, tortuosity, particle size, and distribution [14,32]. Note that loss characteristics are also associated with the porous microstructure, as ionic transport dictates the electrochemical reaction rate [17]. It is noteworthy to mention that capacity, which is a function of applied current and time, is presented with voltage characteristics. Further, it is well known that overpotential significantly contributes to voltage variation. In this context, it can be noted that ohmic overpotential is correlated with ionic pathways on the microstructural scale. Hence, the variation of cell capacity with voltage is illustrated in Fig. 3 for various particle size distributions keeping all the other parameters constant [17]. It is imperative to note that Doyle et al. [17] considered uniform electrode particle size distribution at the anode and cathode, while Taleghani et al. [14] worked with non-uniform particle size distribution at the cathode. It can be seen from Fig. 3 that the non-uniform particle size distribution at the cathode yields a variation in the polarization curve.

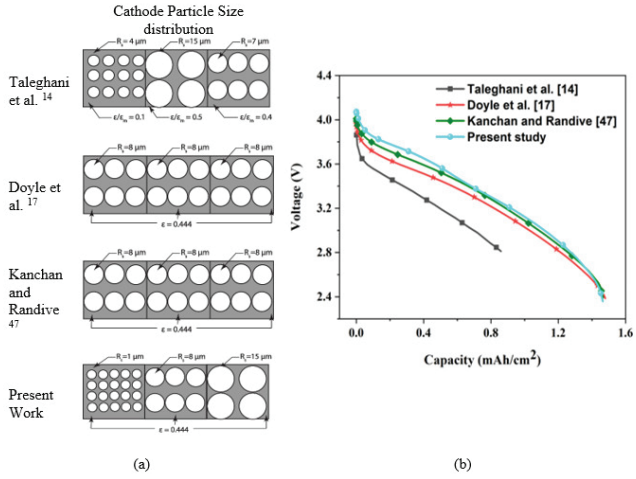

Figure 3: Effect of non-uniform particle size configuration at the cathode: (a) particle size configuration for the cathode, and (b) Improvement in cell capacity.

The promising outcomes of this investigation inspire us to explore the impact of non-uniform cathode particle size distributions on the performance of Li-ion batteries. Such research has the potential to contribute to the development of advanced Li-ion cells through improved design strategies.

5.2 Specific Energy

The specific energy signifies the amount of energy stored for battery mass and significantly influences the gravimetric weight of Li-cell technology [6]. Moreover, it is well established that specific energy depends on cell voltage, which depends on overpotential. Furthermore, the relationship between overpotential and microstructure is noted in ionic transport resistance [5,14]. Hence, variation in specific energy is presented for non-uniform cathode particle size distribution at different current densities, as illustrated in Fig. 4.

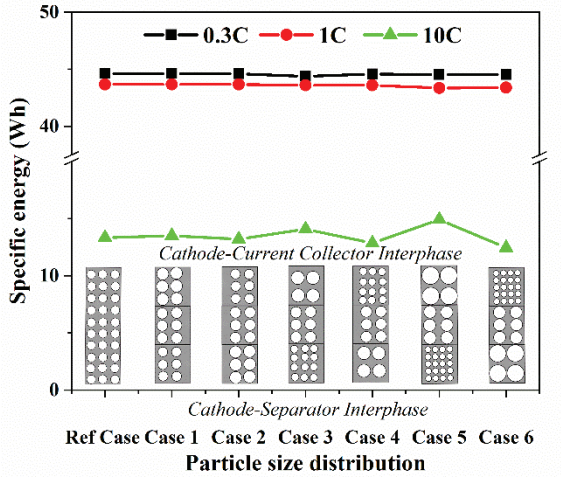

Figure 4: Variation of specific energy for various non-uniform cathode particle distributions at 0.3C, 1C, and 10C.

It is evident from Fig. 4 that specific energy variation is significant at a 10C rate. It is well known that the electrochemical reaction rate is limited by a deficiency of lithium ions at the interstitial sites resulting in slower kinetics through microstructural ionic pathways[6]. When the current density is operated for slow and fast charging-discharging characteristics, the movement of Li-ions is enough to complement the electronic requirements in the interfacial area. On the contrary, ultrafast charging-discharging needs faster ionic and electronic transport. The active material architecture with high electronic conductivity leads to better electronic movement. However, the limitations of microstructure to transport ions are revealed very clearly at a higher C rate since the microstructure's vacancies may not facilitate enough pathways for ionic transport. Hence, the microstructural morphology determines the ionic transport resistance and affects the overall cell performance. Figure 4 also clearly shows that the specific energy increases with an increment in the variation of the cathode particle radius along its length. It is due to the higher interstitial area generated due to variation in non-uniform cathode particle size distribution (refer to Table 2). Higher surface area reduces local current density and exhibits the lowest overpotential [6].

Table 2. Interstitial area considered for different cathode particle size distributions.

Configurations	1st section	2nd section	3rd section
Ref. Case	1.113×10^5	1.113×10^5	1.113×10^5
Case 1	1.272×10^5	1.113×10^5	0.990×10^5
Case 2	0.990×10^5	1.113×10^5	1.272×10^5
Case 3	2.227×10^5	1.113×10^5	0.742×10^5
Case 4	0.742×10^5	1.113×10^5	2.227×10^5
Case 5	8.910×10^5	1.113×10^5	0.594×10^5
Case 6	0.594×10^5	1.113×10^5	8.910×10^5

It can be noted from Table 2 that the cathode particle distribution where particles are increasing along their length (Case 5) has the highest interfacial area near the cathode-separator interphase, which in turn reduces the local current density, and activation overpotential leads to better ionic transport. This active material size distribution resulted in a substantial increase in specific energy by 12% for Case 5, as shown in Fig. 4. On the contrary, the lower interfacial area near the current collector increases local current density and favors electronic transport near the cathode-current collector interphase. When the particle size distribution decreases along the cathode length (Case 6), the specific energy is reduced by 6.6%. It is because Case 6 has the lowest interfacial area near the cathode-separator interphase, which increases the local current density, and activation overpotential restricts ionic transport.

5.3 Specific Power

The specific power signifies how fast energy conversion is feasible between chemical and electrical energy in Li-ion cells [49,50]. Moreover, it is well known that specific power is directly proportional to cell voltage and inversely proportional to time. Further, microstructure topology significantly affects ohmic and activation overpotential when current passes through it. Hence, microstructural topology strongly dominates ionic transport and plays a critical role in determining cell performance [14]. So, the specific power is essential to assess the cell performance for non-uniform cathode particle distribution, as shown in Fig. 5. The value of specific power increases with an increment in the C-rate irrespective of the cathode particle configuration. This

observation is consistent with earlier work established by researchers [36,37]. Furthermore, Fig. 5 also illustrates that the specific power value remains constant for 0.3C and 1C with cathode particle configurations. The ionic transport at low current densities is not limited due to microstructural morphology as the ionic flux requirement is low, and even the ionic transport encounters multiple resistance. Still, the time given to reach the ionic flux for the electrochemical reaction is sufficient. Additionally, Fig. 5 shows that the value of specific power significantly varies for cathode particle configuration at 10C. This is intuitive since the ionic flux requirement is significantly large at a higher C-rate. Moreover, ionic transport is strongly dependent on microstructural morphology. In addition, variation in particle size results in different interfacial areas, and therefore, the local current density varies, which in turn affects the overpotential. Figure 5 depicts the maximum specific power for the cathode particle distribution where particles increase along their length (Case 5). This is basically due to its particle configuration, which shows a higher interfacial area at the cathode-separator interphase to promote ionic transport. The higher interfacial area lowers local current density and activation overpotential [6].

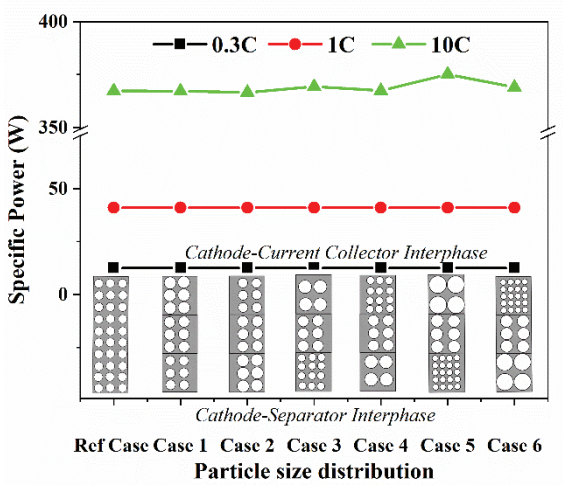

Figure 5. Variation of specific power for various non-uniform cathode particle distributions at 0.3C, 1C, and 10C.

Moreover, a lower interfacial area at the cathode-current collector interphase promotes electronic transport. The lower interfacial area signifies the active material presence, which is a pathway for electronic transport. The higher the active material presence, the lower the ohmic resistance, facilitating electron movement near the cathode-current collector interphase since it primarily deals with electronic transport.

5.4 Capacity

The presence of non-uniform electrode microstructures directly impacts ionic transport and, consequently, influences the cell's overall performance [6,51–54]. To illustrate the effects of non-uniform cathode particle configurations, the polarization curve is depicted in Figure 6, considering slow, fast, and ultrafast current densities. Upon examining Figures 6(a)-(b), it becomes evident that the discharge and charge behavior remains relatively stable at low current density (0.3C). This constancy is attributed to the fact that slow ionic transport has minimal influence on the overall ionic transport requirement, as the time required for ionic transport is significantly high. A little variation in the polarization curve is observed at 1C in Figs. 6(c)-(d) shows some variation in the particle size distribution. The influence of microstructural morphology on ion transport becomes more prominent at higher current density (10C). As a result, the impact of non-uniform cathode particle distribution is clearly noticeable in both the discharging and charging behavior at 10C, as depicted in Figures 6(e)-(f). Note that when particle size increases along the cathode length (Case 5), the highest capacity for discharging and charging is observed due to a higher interfacial area near the cathode-separator interphase. On the contrary, poor performance is observed with the lowest capacity when particle size reduces along the length of the cathode (Case 6). Moreover, the deviation in cell performance is significant for Case 5 and Case 6 at a higher C-rate. Hence, the effect of these two particle size distributions (Case 5 and Case 6) is investigated in detail for electrochemical loss characteristics in the subsequent section.

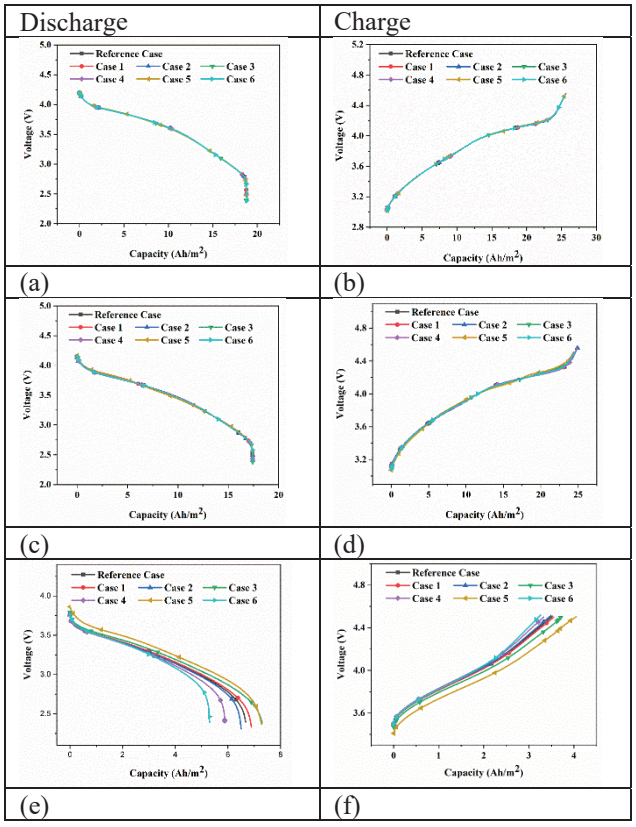

Figure 6: Polarization curve: Effect of non-uniform cathode particle distribution (a)–(b) 0.3C, (c)–(d) 1C, and (e) – (f) 10C.

5.5 Loss Characteristics: Overpotential & Power Dissipation Density

It is essential to study the loss characteristics to understand the transport constraints for various non-uniform cathode microstructural topologies [55] since the overpotential and total power dissipation density best describes the electrochemical loss characteristics in Li-ion cells [56], its temporal variation for different non-uniform particle configurations is presented and discussed in the subsequent section.

5.5.1. Overpotential

The overpotential characterizes the various losses in terms of activation energy, internal resistance, and concentration gradient, depending on electrode morphology. It can be noted that overpotential characteristics are vital in understanding the relationship between different non-uniform particle configurations and cell performance [55,57]. Therefore, the variation of overpotential is illustrated for different non-uniform cathode particle configurations.

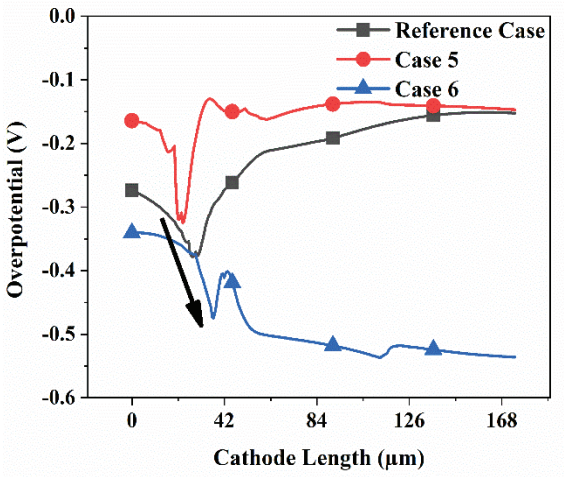

Figure 7: Overpotential variation for non-uniform cathode particle distribution at 10C.

Figure 7 shows a sudden overpotential increment near the cathode separator interphases irrespective of the particle size distributions considered due to ionic transport limitation occurring near the cathode separator interphase. Thereafter a sharp decrease in overpotential followed, which is consistent with earlier work reported by researchers [6,40]. Furthermore, it is evident from Fig. 7 that the overpotential is minimum when particle size increases along the electrode length (Case 5) since the higher interfacial area near the cathode-separator interphase and the lower interfacial area near the cathode-current collector interphase facilitates the ionic transport and electronic transport respectively, thus reducing the activation and ohmic overpotential. On the contrary, overpotential is maximum when the interfacial area near the cathode-separator interphase is lesser than the cathode-current collector interphase area. It can also be noted that a significant increment in overpotential is observed when particle size decreases along the cathode length (Case 6) near the cathode-current collector interphase as it has a higher interstitial area, which leads to higher activation and ohmic overpotential.

5.5.2. Power dissipation density

Power dissipation density depicts the total reversible and non-reversible loss in the cell operation. Note that the microstructure aspect of the electrode can be useful for assessing active material and pore distribution, which can be customized to minimize loss [56]. Hence, the influence of non-uniform cathode particle size distribution is shown on power dissipation density is plotted. Figure 8 illustrates that power dissipation density increases with time for all the cases considered. It is attributed to the fact that losses are generated, and since these losses are primarily exothermic, the power dissipation density increases with time. Figure 8 shows that the lowest power dissipation density is observed when particle size increases along the cathode length (Case 5). It is due to higher ionic transport architecture with the higher interfacial area near the cathode-separator interphase and the lower interfacial area near the cathode-current collector. Higher interfacial area reduces local current density, reducing overpotential and power dissipation.

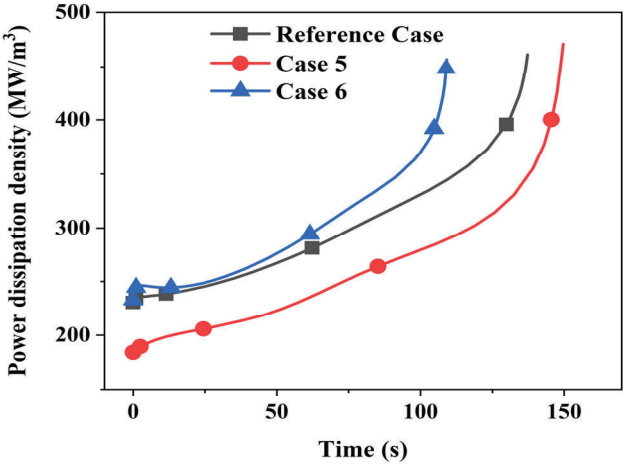

Figure 8: Variation of power dissipation density for non-uniform cathode particle distribution at 10C

In contrast, Fig. 8 shows that the highest power dissipation density is observed in Case 6. Its particle size configuration leads to a lower interfacial area near the cathode-separator interphase and a higher interfacial area near the cathode-current collector. Lower interfacial area leads to an increment in local current density and thereby increases over-potential and power dissipation density.

6. CONCLUSIONS

This study examines how non-uniform distributions of cathode particle sizes affect lithium-ion batteries' charging and discharging characteristics, specifically during slow, fast, and ultrafast processes. Various non-uniform cathode configurations have been thoroughly analyzed in this research based on particle size and distribution to gain insight into capacity, specific energy, specific power, overpotential, and power dissipation density. The specific findings of the study are given below:

- Non-uniform particle size distribution along the cathode affects cell performance. The cell performance is observed better when the distribution of non-uniform particle size is employed compared to the uniform particle size distribution. The gain in cell performance parameters increases with the increase in C-rate, and particle size grows at a higher rate along the cathode length.
- Specific energy, specific power, and capacity are found to be maximum when cathode particle distribution increases particle size along the cathode length (Case 5). On the contrary, the specific energy, specific power, and capacity are found to be the least when cathode particle distribution decreases particle size along the cathode length (Case 6).
- Loss characteristics, viz. overpotential and power dissipation density, confirm that losses are minimal when the size of the cathode particle increases along the length (Case 5). On the contrary, losses are maximum when the

size of the cathode particle decreases along the length (Case 6)

- Although the sharp increment in the value of overpotential is observed near the cathode separator interphase irrespective of particle size distribution, the length along the cathode at which this variation occurs depends on particle size distribution.

REFERENCES

[1] Messerli, P., Murniningtyas, E. (2019). Global Sustainable Development Report: The Future is Now – Science for Achieving Sustainable Development. vol. 1. New York.

[2] Lin, J., Liu, X., Li, S., Zhang, C., Yang, S. (2021). A review on recent progress, challenges and perspective of battery thermal management system. Int J Heat Mass Transf 2021;167:120834. https://doi.org/10.1016/j.ijheatmasstransfer.2020.120834

[3] Zubi, G., Dufo-López, R., Carvalho, M., Pasaoglu, G. (2018). The lithium-ion battery: State of the art and future perspectives. Renew Sustain Energy Rev 2018;89:292–308. https://doi.org/10.1016/j.rser.2018.03.002.

[4] Jiang X, Chen Y, Meng X, Cao W, Liu C, Huang Q, et al. (2022). The impact of electrode with carbon materials on safety performance of lithium-ion batteries: A review. Carbon N Y 2022;191:448–70. https://doi.org/10.1016/j.carbon.2022.02.011.

[5] Mistry, A.N., Smith, K., Mukherjee, P.P. (2018). Secondary-Phase Stochastics in Lithium-Ion Battery Electrodes. ACS Appl Mater Interfaces 2018;10:6317–26. https://doi.org/10.1021/acsami.7b17771.

[6] Reddy, T., Linden, D. (2011). Linden's Handbook of batteries. 4th ed. The McGraw-Hill Companies.

[7] Liu, Y., Zhu, Y., Cui, Y. (2019). Challenges and opportunities towards fast-charging battery materials. Nat Energy 2019;4:540–50. https://doi.org/10.1038/s41560-019-0405-3.

[8] Walter, M., Kovalenko, M.V., Kravchyk, K.V. (2020). Challenges and benefits of post-lithium-ion batteries. New J Chem 2020;44:1677–83. https://doi.org/10.1039/c9nj05682c.

[9] Ue, M,, Sakaushi, K., Uosaki, K. (2020). Basic knowledge in battery research bridging the gap between academia and industry. Mater Horizons 2020;7:1937–54. https://doi.org/10.1039/d0mh00067a.

[10] Masoudi, R., Uchida. T., McPhee, J. (2015). Parameter estimation of an electrochemistry-based lithium-ion battery model. J Power Sources 2015;291:215–24. https://doi.org/10.1016/j.jpowsour.2015.04.154.

[11] Chen, C.H., Brosa-Planella, F., O'Regan, K., Gastol, D., Widanage, W.D., Kendrick, E. (2020). Development of Experimental Techniques for Parameterization of Multi-scale Lithium-ion Battery Models. J Electrochem Soc 2020;167:080534. https://doi.org/10.1149/1945-7111/ab9050.

[12] Agubra, V., Fergus, J. (2013). Lithium ion battery anode aging mechanisms. Materials (Basel) 2013;6:1310–25. https://doi.org/10.3390/ma6041310.

[13] Joho, F., Rykart, B., Blome, A., Novák, P., Wilhelm, H., Spahr, M.E. (2001). Relation between surface properties, pore structure and first-cycle charge loss of graphite as negative electrode in lithium-ion batteries. J Power Sources 2001;97–98:78–82. https://doi.org/10.1016/S0378-7753(01)00595-X.

[14] Taleghani, S.T., Marcos, B., Zaghib, K., Lantagne, G. (2017). A Study on the Effect of Porosity and Particles Size Distribution on Li-Ion Battery Performance. J Electrochem Soc 2017;164:E3179–89. https://doi.org/10.1149/2.0211711jes.

[15] Fuller, T.F., Doyle, M., Newman, J. (1994). Simulation and Optimization of the Dual Lithium Ion Insertion Cell. J Electrochem Soc 1994;141:1–10. https://doi.org/10.1149/1.2054684.

[16] Das, M.K., Mukherjee, P.P., Muralidhar, K. (2018). Porous Media Applications: Biological Systems 2018:123–54. https://doi.org/10.1007/978-3-319-69866-3_5.

[17] Doyle, M., Newman, J., Gozdz, A.S., Schmutz, C.N., Tarascon, J. (1996). Comparison of Modeling Predictions with Experimental Data from Plastic Lithium Ion Cells. J Electrochem Soc 1996;143:1890–903. https://doi.org/10.1149/1.1836921.

[18] Doyle, M., Fuller, T.F., Newman, J. (1993). Modeling of Galvanostatic Charge and Discharge. J Electrochem Soc 1993;140:1526–33.

[19] Darling, R., Newman, J. (1997). Modeling a Porous Intercalation Electrode with Two Characteristic Particle Sizes. J Electrochem Soc 1997;144:4201–8. https://doi.org/10.1149/1.1838166.

[20] Baade, P., Ebner, M., Wood, V. (2017). Rapid, Non-Invasive Method for Quantifying Particle Orientation Distributions in Graphite Anodes. J Electrochem Soc 2017;164:E348–51. https://doi.org/10.1149/2.1291712jes.

[21] Hosseinzadeh, E., Marco, J., Jennings, P. (2017). Electrochemical-thermal modelling and optimisation of lithium-ion battery design parameters using analysis of variance. Energies 2017;10. https://doi.org/10.3390/en10091278.

[22] Bae, C.J., Erdonmez, C.K., Halloran, J.W., Chiang, Y.M. (2013). Design of battery electrodes with dual-scale porosity to minimize tortuosity and maximize performance. Adv Mater 2013;25:1254–8. https://doi.org/10.1002/adma.201204055.

[23] Wood, V., Ebner, M.O.J. (2014). Method for the production of electrodes and electrodes made using such a method.

[24] Billaud, J., Bouville, F., Magrini, T., Villevieille, C., Studart, A.R. (2016). Magnetically aligned graphite electrodes for high-rate performance Li-ion batteries. Nat Energy 2016;1:1–6. https://doi.org/10.1038/nenergy.2016.97.

[25] Peterson, S.W., Wheeler, D.R. (2014). Direct Measurements of Effective Electronic Transport in Porous Li-Ion Electrodes. J Electrochem Soc 2014;161:A2175–81. https://doi.org/10.1149/2.0661414jes.

[26] Ramadesigan, V., Methekar, R.N., Latinwo, F., Braatz, R.D., Subramanian, V.R. (2010). Optimal Porosity Distribution for Minimized Ohmic Drop across a Porous Electrode. J Electrochem Soc 2010;157:A1328. https://doi.org/10.1149/1.3495992.

[27] Hur, J.I., Smith, L.C., Dunn, B. (2018). High Areal Energy Density 3D Lithium-Ion Microbatteries. Joule

2018;2:1187–201. https://doi.org/10.1016/j.joule.2018.04.002.
[28] Pikul, J.H., Gang, Z.H., Cho, J., Braun, P.V., King, W.P. (2013). High-power lithium ion microbatteries from interdigitated three-dimensional bicontinuous nanoporous electrodes. Nat Commun 2013;4:1–5. https://doi.org/10.1038/ncomms2747.
[29] Suthar, B., Northrop, P.W.C., Rife, D., Subramanian, V.R. (2015). Effect of Porosity, Thickness and Tortuosity on Capacity Fade of Anode. J Electrochem Soc 2015;162:A1708–17. https://doi.org/10.1149/2.0061509jes.
[30] Liu, R., Duay, J., Lee, S.B. (2011). Heterogeneous nanostructured electrode materials for electrochemical energy storage. Chem Commun 2011;47:1384–404. https://doi.org/10.1039/c0cc03158e.
[31] Park, C.M., Sohn, H.J. (2008). Tetragonal zinc diphosphide and its nanocomposite as an anode for lithium secondary batteries. Chem Mater 2008;20:6319–24. https://doi.org/10.1021/cm800632f.
[32] Bläubaum, L., Röder, F., Nowak, C., Chan, H.S., Kwade, A., Krewer, U. (2020). Impact of Particle Size Distribution on Performance of Lithium-Ion Batteries. ChemElectroChem 2020;7:4755–66. https://doi.org/10.1002/celc.202001249.
[33] Park, Y.S., Lee, S.M. (2009). Effects of particle size on the thermal stability of lithiated graphite anode. Electrochim Acta 2009;54:3339–43. https://doi.org/10.1016/j.electacta.2008.12.030.
[34] Von, S.U., Nodwell, E., Sundher, A., Dahn, J.R. (1995). Comparative thermal stability of carbon intercalation anodes and lithium metal anodes for rechargeable lithium batteries. J Power Sources 1995;54:240–5. https://doi.org/10.1016/0378-7753(94)02076-F.
[35] Tran, T.D., Feikert, J.H., Pekala, R.W., Kinoshita, K. (1996). Rate effect on lithium-ion graphite electrode performance. J Appl Electrochem 1996;26:1161–7. https://doi.org/10.1007/BF00243741.
[36] Meyer, M., Komsiyska, L., Lenz, B., Agert, C. (2013). Study of the local SOC distribution in a lithium-ion battery by physical and electrochemical modeling and simulation. Appl Math Model 2013;37:2016–27. https://doi.org/10.1016/j.apm.2012.04.029.
[37] Ali, Y., Iqbal, N., Lee, S. (2020). Simultaneous effect of particle size and location on stress development in the electrodes of lithium-ion batteries. Int J Energy Res 2020;44:12145–57. https://doi.org/10.1002/er.5795.
[38] Du, W., Gupta, A., Zhang, X., Sastry, A.M., Shyy, W. (2010). Effect of cycling rate, particle size and transport properties on lithium-ion cathode performance. Int J Heat Mass Transf 2010;53:3552–61. https://doi.org/10.1016/j.ijheatmasstransfer.2010.04.017.
[39] Kespe, M., Cernak, S., Gleiß, M., Hammerich, S., Nirschl, H. (2019). Three-dimensional simulation of transport processes within blended electrodes on the particle scale. Int J Energy Res 2019;43:6762–78. https://doi.org/10.1002/er.4616.
[40] Azami-Ghadkolai, M., Yousefi, M., Allu, S., Creager, S., Bordia, R. (2020). Effect of isotropic and anisotropic porous microstructure on electrochemical performance of Li ion battery cathodes: An experimental and computational study. J Power Sources 2020;474:228490. https://doi.org/10.1016/j.jpowsour.2020.228490.
[41] Liang, Z., Yan, K., Zhou, G., Pei, A., Zhao, J., Sun, Y., et al. (2019). Composite lithium electrode with mesoscale skeleton via simple mechanical deformation. Sci Adv 2019;5:1–9. https://doi.org/10.1126/sciadv.aau5655.
[42] Pomerantseva, E., Bonaccorso, F., Feng, X., Cui, Y., Gogotsi, Y. (2019). Energy storage: The future enabled by nanomaterials. Science (80-) 2019;366. https://doi.org/10.1126/science.aan8285.
[43] Li, X., Gu, M., Hu, S., Kennard, R., Yan, P., Chen, X., et al. (2014). Mesoporous silicon sponge as an anti-pulverization structure for high-performance lithium-ion battery anodes. Nat Commun 2014;5. https://doi.org/10.1038/ncomms5105.
[44] Xia, Y., Zhao, T., Zhu, X., Zhao, Y., He, H., Hung, C. et al. (2021). Inorganic-organic competitive coating strategy derived uniform hollow gradient-structured ferroferric oxide-carbon nanospheres for ultra-fast and long-term lithium-ion battery. Nat Commun 2021;12:1–10. https://doi.org/10.1038/s41467-021-23150-8.
[45] Dai, H., Jiang, B., Hu, X., Lin, X., Wei, X., Pecht, M. (2021). Advanced battery management strategies for a sustainable energy future: Multilayer design concepts and research trends. Renew Sustain Energy Rev 2021;138:110480. https://doi.org/10.1016/J.RSER.2020.110480.
[46] Sulzer, V., Mohtat, P., Aitio, A., Lee, S., Yeh, Y.T., Steinbacher, F., et al. (2021). The challenge and opportunity of battery lifetime prediction from field data. Joule 2021;5:1934–55. https://doi.org/10.1016/j.joule.2021.06.005.
[47] Kanchan, B.K., Randive, P.R. (2021). Implication of Non-Uniform Anode Particle Morphology on Lithium-Ion Cell Performance. J Electrochem Soc 2021;168:050552. https://doi.org/10.1149/1945-7111/ac035a.
[48] Appiah, W.A., Ryou, M.H., Lee, Y.M. (2019). A Physics-Based Model Capacity Fade Analysis of LiMn 2 O 4 /Graphite Cell at Different Temperatures . J Electrochem Soc 2019;166:A5109–16. https://doi.org/10.1149/2.0161903jes.
[49] Smith, K., Wang, C.Y. (2006). Power and thermal characterization of a lithium-ion battery pack for hybrid-electric vehicles. J Power Sources 2006;160:662–73. https://doi.org/10.1016/j.jpowsour.2006.01.038.
[50] Zhang, B., Su, D. (2022). Battery Thermal Management and Health State Assessment of New Energy Vehicles. International Journal of Heat and Technology 2022; 40:2: 653-659. https://doi.org/10.18280/ijht.400237
[51] Crompton, T.R. (2000). Battery reference book. 3rd ed. Oxford: Newnes; . https://doi.org/10.5860/choice.28-1573.
[52] Hariharan, K.S., Tagade, P., Ramachandran, S. (2018). Mathematical Modeling of Lithium Batteries. 1st ed. Bangalore: Springer; . https://doi.org/https://doi.org/10.1007/978-3-319-03527-7.
[53] Soge, A.O.,Willoughby, A.A.,Dairo, O.F.,Onatoyinbo, O.O. (2021). Cathode Materials for Lithium-ion Batteries : A brief review. Journal of New Materials for Electrochemical Systems 2021;24:4: 229-246. https://doi.org/10.14447/jnmes.v24i4.a02
[54] Kumar, R.,Chavan, S. (2022). Numerical and Experimental Investigation of Thermal Behaviour for

Fast Charging and Discharging of Various 18650 Lithium Batteries of Electric Vehicles. International Journal of Heat and Technology 2022;40:6: 1492-1499. https://doi.org/10.18280/ijht.400618

[55] Newman, J., Thomas-Alyea, K.E. (2004). Electrochemical Systems. 3rd ed. New Jersey: Wiley-Interscience.

[56] Kanchan, B.K., Randive, P.R., Pati, S. (2021). On the Implication of Porosity Configuration on Lithium-Ion Cell Performance: A Numerical Study. J Electrochem Energy Convers Storage 2021;18. https://doi.org/10.1115/1.4046754.

[57] Chen, Z., Danilov, D.L., Raijmakers, L.H.J., Chayambuka, K., Jiang, M., Zhou, L., et al. (2021). Overpotential analysis of graphite-based Li-ion batteries seen from a porous electrode modeling perspective. J Power Sources 2021;509:230345. https://doi.org/10.1016/J.JPOWSOUR.2021.230345.